

Unmasking Anomalies in Road-Scene Segmentation

Original

Unmasking Anomalies in Road-Scene Segmentation / Rai, S.N., Cermelli, F., Fontanel, D., Masone, C., Caputo, B.. - (2023), pp. 4014-4023. (International Conference on Computer Vision 2023 Paris (FR) 01-06 October 2023) [10.1109/ICCV51070.2023.00373].

Availability:

This version is available at: 11583/2982324 since: 2023-09-19T21:53:10Z

Publisher:

IEEE

Published

DOI:10.1109/ICCV51070.2023.00373

Terms of use:

This article is made available under terms and conditions as specified in the corresponding bibliographic description in the repository

Publisher copyright

(Article begins on next page)

Unmasking Anomalies in Road-Scene Segmentation

Shyam Nandan Rai¹, Fabio Cermelli^{1,2}, Dario Fontanel¹, Carlo Masone¹, Barbara Caputo¹
¹Politecnico di Torino, ²Italian Institute of Technology

first.last@polito.it

Abstract

Anomaly segmentation is a critical task for driving applications, and it is approached traditionally as a per-pixel classification problem. However, reasoning individually about each pixel without considering their contextual semantics results in high uncertainty around the objects' boundaries and numerous false positives. We propose a paradigm change by shifting from a per-pixel classification to a mask classification. Our mask-based method, Mask2Anomaly, demonstrates the feasibility of integrating an anomaly detection method in a mask-classification architecture. Mask2Anomaly includes several technical novelties that are designed to improve the detection of anomalies in masks: i) a global masked attention module to focus individually on the foreground and background regions; ii) a mask contrastive learning that maximizes the margin between an anomaly and known classes; and iii) a mask refinement solution to reduce false positives. Mask2Anomaly achieves new state-of-the-art results across a range of benchmarks, both in the per-pixel and component-level evaluations. In particular, Mask2Anomaly reduces the average false positives rate by 60% w.r.t. the previous state-of-the-art. Github page: <https://tinyurl.com/54ydrxvj>

1. Introduction

Semantic segmentation [14, 45, 54, 52, 46] plays a significant role in self-driving cars because it provides a detailed understanding of surroundings. Generally, semantic segmentation models are trained to recognize a pre-defined set of semantic classes (e.g. car, pedestrian, road, etc.); however, in real-world applications, they may encounter objects not belonging to such categories (e.g. animals or cargo dropped on the road). Therefore, it is essential for these models to identify objects in a scene that are not present during training *i.e.* anomalies, both to avoid potential dangers and to enable continual learning [39, 8, 17, 7] and open-world solutions [6].

Anomaly segmentation (AS) [3, 51, 20, 27] addresses this problem, *i.e.* it aims to segment objects from classes

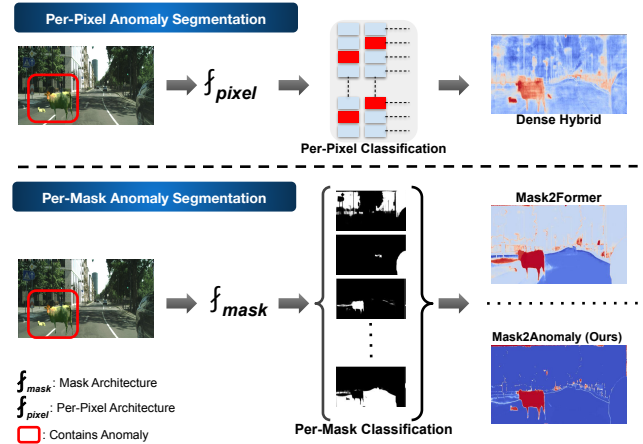


Figure 1: **Per-pixel vs per-mask Anomaly Segmentation:** Dense Hybrid [22], the state-of-the-art method for AS based on per-pixel classification can detect the anomalies, but it produces many false positives. Anomaly segmentation can be cast as a mask classification problem, but naively using MSP [25] on top of Mask2Former [12] does not produce good results. Our Mask2Anomaly exploits mask-transformers properties to refine the classification of anomalies, drastically reducing false positives. f_{pixel} and f_{mask} denotes per-pixel, and per-mask architecture. Anomalies in the output image are represented in red.

that were absent during training. Existing AS methods are built upon the idea of individually classifying the pixels and assigning to each of them an anomaly score. This score may be given by a pixel-level discriminative method [1, 27, 22, 47], by estimating the uncertainty of the individual pixel predictions [41], or by comparing the per-pixel discrepancy between the original image and a synthetic image generated from the semantic predictions [34, 49, 50]. However, reasoning on the pixels individually produces noisy anomaly scores, thus leading to a high number of false positives and poorly localized anomalies (see Fig. 1).

In this paper, we propose to address this problem by casting AS as a mask classification task rather than a pixel classification. This idea stems from the recent advances

in mask-transformer architectures [12, 13], which demonstrated that it is possible to achieve remarkable performance across various segmentation tasks by classifying masks, rather than pixels. We hypothesize that mask-transformer architectures are better suited to detect anomalies than per-pixel architectures [11, 26], because masks encourage objectness and thus can capture anomalies as whole entities, leading to more congruent anomaly scores and reduced false positives. To enable the segmentation of anomalies at the mask level, we revisit the Maximum Softmax Probability (MSP) [25], a classic method used in per-pixel AS, and apply it to the masks produced by a mask-transformer model. However, the effectiveness of such an approach hinges on the model’s capability to output masks that capture well anomalies and we found that naively using MSP on top of the best mask-transformer architecture [12] does not yield good results (see Fig. 1). Hence, we propose several technical contributions to improve the capability of mask-transformer architectures to capture anomalies and reject false positives in driving scenes (see Fig. 1):

- At the **architectural** level, we propose a global masked-attention mechanism that allows the model to focus on both the foreground objects and on the background while retaining the efficiency of the original masked-attention [12].
- At the **training** level, we have developed a mask contrastive learning framework that utilizes outlier masks from additional out-of-distribution data to maximize the separation between anomalies and known classes.
- At the **inference** level, we propose a mask-based refinement solution that reduces false positives by filtering masks based on the panoptic segmentation [28] that distinguishes between “things” and “stuff”.

We integrate these contributions on top of the mask architecture [12] and term this solution **Mask2Anomaly**. To the best of our knowledge, Mask2Anomaly is the first demonstration of an AS method that detects anomalies at the mask level. We tested Mask2Anomaly on standard anomaly segmentation benchmarks for road scenes (Road Anomaly [34], Fishyscapes [4], Segment Me If You Can [9]), achieving the best results among all AS methods by a significant margin. In particular, Mask2Anomaly reduces on average the false positives rate by more than half w.r.t. the previous state-of-the-art. Code and pre-trained models will be made publicly available upon acceptance.

2. Related Work

Mask-based semantic segmentation. Traditionally, semantic segmentation methods [37, 11, 56, 32, 55] have adopted fully-convolutional encoder-decoder architectures [37, 2] and addressed the task as a dense classification problem. However, transformer architectures have recently

caused us to question this paradigm due to their outstanding performance in closely related tasks such as object detection [5] and instance segmentation [23]. In particular, [13] proposed a mask-transformer architecture that addresses segmentation as a mask classification problem. It adopts a transformer and a per-pixel decoder on top of the feature extraction. The generated per-pixel and mask embeddings are combined to produce the segmentation output. Building upon [13], [12] introduced a new transformer decoder adopting a novel masked-attention module and feeding the transformer decoder with one pixel-decoder high-resolution feature at a time.

So far, all these mask-transformers have been considered exclusively in a closed set setting, i.e, there are no unknown categories at test time. To the best of our knowledge, Mask2Anomaly is the first method that performs AS directly with mask-transformers, thus empowering these approaches with the capability to recognize anomalies in real-world settings.

Anomaly segmentation methods can be broadly divided into three categories: (a) Discriminative, (b) Generative, and (c) Uncertainty-based methods. *Discriminative Methods* are based on the classification of the model outputs. Hendrycks and Gimpel [25] established the initial AS discriminative baseline by applying a threshold over the maximum softmax probability (MSP) that distinguishes between in-distribution and out-of-distribution data. Other approaches use auxiliary datasets to improve performance [31, 27, 47] by calibrating the model over-confident outputs. Alternatively, [30] learns a confidence score by using the Mahalanobis distance, and [10] introduces an entropy-based classifier to discover out-of-distribution classes. Recently, discriminative methods tailored for semantic segmentation [4] directly segment anomalies in embedding space. In contrast, [22] proposes a hybrid approach that combines the known class posterior, dataset posterior, and an un-normalized data likelihood to estimate anomalies. *Generative Methods* provides an alternative paradigm to segment anomalies based on generative models [34, 16, 50, 49]. These approaches train generative networks to reconstruct anomaly-free training data and then use the generation discrepancy to detect an anomaly at test time. All the generative-based methods heavily rely on the generation quality and thus experience performance degradation due to image artifacts [20]. Finally, *Uncertainty based* methods segment anomalies by leveraging uncertainty estimates via Bayesian neural networks [41].

All the methods discussed above are based on per-pixel classification architectures and score the pixels individually without considering local semantics, leading to noisy anomaly predictions and many false positives. Mask2Anomaly overcomes this limitation by segmenting anomalies as semantically clustered masks, encouraging the

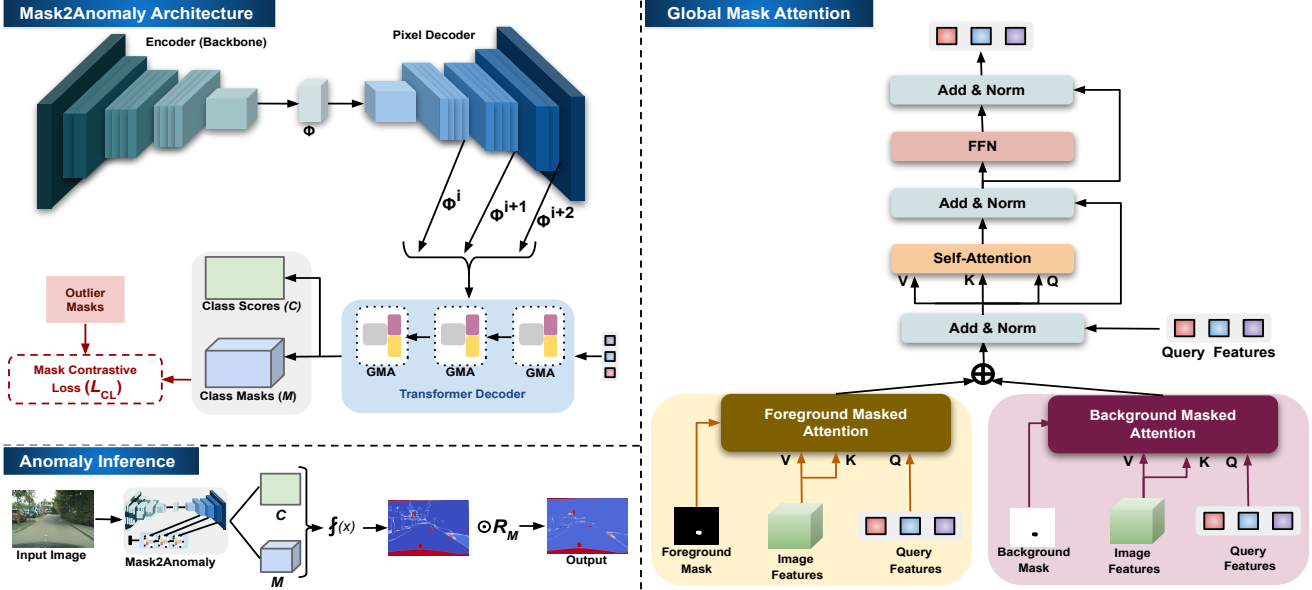


Figure 2: **Mask2Anomaly Overview.** Mask2Anomaly meta-architecture consists of an encoder, a pixel decoder, and a transformer decoder. We propose global mask attention (Sec. 3.2) that independently distributes the attention between foreground and background. V , K , and Q are Value, Key, and Query. ϕ is image features. $\phi^i, \phi^{i+1}, \phi^{i+2}$ are upsampled image features at multiple scales. Mask contrastive Loss L_{CL} (Sec. 3.3) utilizes outlier masks to maximize the separation between anomalies and known classes. During anomaly inference, we utilize refinement mask R_M (Sec. 3.4) to minimize false positives.

objectness of the predictions. To the best of our knowledge, this is the first work to use masks to score anomalies.

3. Method

In this section, we begin by introducing problem-setting, followed by describing a generic mask-transformer architecture for anomaly segmentation. Next, we delve into our Mask2Anomaly architecture and its novel elements.

3.1. Preliminaries

Let us denote with $\mathcal{X} \subset \mathbb{R}^{3 \times H \times W}$ the space of RGB images, where H and W are the height and width, respectively, and with $\mathcal{Y} \subset \mathbb{N}^{K \times H \times W}$ the space of semantic labels that associate each pixel in an image to a semantic category from a predefined set \mathcal{K} , with $|\mathcal{K}| = K$. At training time we assume to have a dataset $\mathcal{D} = \{(x_i, y_i)\}_{i=1}^D$, where $x_i \in \mathcal{X}$ is an image and $y_i \in \mathcal{Y}$ is its ground truth semantic mask. The goal for an anomaly segmentation model is to learn a function f that maps the image space to an anomaly score space, i.e. $f : \mathcal{X} \mapsto \mathbb{R}^{H \times W}$. For traditional semantic segmentation architectures based on per-pixel classification [11], the function f can be obtained in various ways, for example, applying the *Maximum Softmax Probability* (MSP) [25] on top of the per-pixel classifier. Formally, given the pixel-wise class scores $S(x) \in [0, 1]^{K \times H \times W}$ obtained by segmenting the image x with a per-pixel architec-

ture, we compute the anomaly score as:

$$f(x) = 1 - \max_{k=1}^K (S(x)). \quad (1)$$

In this paper, we propose to adapt this framework based on MSP to mask-transformer segmentation architectures. We recall that the mask classification problem is formulated as a direct set prediction task with the goal of producing a fixed-size set of N predictions [5]. Based on this idea, the mask classification meta-architecture for semantic segmentation consists of three parts: a) a *backbone* that acts as feature extractor, b) a *pixel-decoder* that upsamples the low-resolution features extracted from the backbone to produce high-resolution *per-pixel embeddings*, and c) a *transformer decoder*, made of L transformer layers, that takes the image features to output a fixed number of object queries consisting of *mask embeddings* and their associated *class scores* $C \in \mathbb{R}^{N \times K}$. The final *class mask* $M \in \mathbb{R}^{N \times (H \times W)}$ are obtained by multiplying the mask embeddings with the per-pixel embeddings. The mask-transformer is trained using a combination of binary cross-entropy loss and dice loss [40] for the class masks and cross-entropy loss for the class scores, unlike per-pixel architecture that is trained only on cross-entropy loss (more details on these losses are given in the supplementary material).

Given such a mask-transformer architecture, we propose



Figure 3: **Limitation of Mask-Attention:** Masked-attention [12] selectively attends to foreground regions resulting in low attention scores (dark regions) for anomalies. Anomalies are in red. Best viewed with zoom.

to calculate the anomaly scores for an input x as

$$f(x) = 1 - \max_{k=1}^K (\text{softmax}(C)^T \cdot \text{sigmoid}(M)). \quad (2)$$

Here, $f(x)$ utilizes the same marginalization strategy of class and mask pairs as [13] to get anomaly scores. Without loss of generality, we implement the anomaly scoring (Eq. (2)) on top of the Mask2Former [12] architecture. However, this strategy hinges on the fact that the masks predicted by the segmentation architecture can capture anomalies well. We found that simply applying the MSP on top of Mask2Former as in Eq. (2) does not yield good results (see Fig. 1 and the results in Sec. 4.2). To overcome this problem, we introduce improvements in the architecture, training procedure, and anomaly inference mechanism. We name our method as Mask2Anomaly, and its overview is shown in Fig. 2 (left). In the rest of the sections, we will discuss in detail the technical novelties of Mask2Anomaly.

3.2. Global Masked Attention

One of the key ingredients to Mask2Former [12] state-of-the-art segmentation results is the replacement of the *cross-attention* (CA) layer in the transformer decoder with a *masked-attention* (MA). The masked-attention attends only to pixels within the foreground region of the predicted mask for each query, under the hypothesis that local features are enough to update the query object features. The output of the l -th masked-attention layer can be formulated as

$$\text{softmax}(\mathcal{M}_l^F + QK^T)V + X_{in} \quad (3)$$

where $X_{in} \in \mathbb{R}^{N \times C}$ are the N C -dimensional query features from the previous decoder layer. The input queries $Q \in \mathbb{R}^{N \times C}$ are obtained by linearly transforming the query features with a learnable transformation whereas the keys and values K, V are the image features under learnable linear transformations $f_k(\cdot)$ and $f_v(\cdot)$. Finally, \mathcal{M}_l^F is the predicted foreground attention mask that at each pixel location (i, j) is defined as

$$\mathcal{M}_l^F(i, j) = \begin{cases} 0 & \text{if } M_{l-1}(i, j) \geq 0.5 \\ -\infty & \text{otherwise,} \end{cases} \quad (4)$$

where M_{l-1} is the output mask of the previous layer.

By focusing only on the foreground objects, masked-attention grants faster convergence and better semantic segmentation performance than cross-attention. However, focusing only on the foreground region constitutes a problem for anomaly segmentation because anomalies may also appear in the background regions. Removing background information leads to failure cases in which the anomalies in the background are entirely missed, as shown in the example in Fig. 3. To ameliorate the detection of anomalies in these corner cases, we extend the masked attention with an additional term focusing on the background region (see Fig. 2, right). We call this a *global masked-attention* (GMA) formally expressed as

$$X_{out} = \text{softmax}(\mathcal{M}_l^F + QK^T)V + \text{softmax}(\mathcal{M}_l^B + QK^T)V + X_{in} \quad (5)$$

where \mathcal{M}_l^B is the additional background attention mask that complements the foreground mask \mathcal{M}_l^F , and it is defined at the pixel coordinates (i, j) as

$$\mathcal{M}_l^B(i, j) = \begin{cases} 0 & \text{if } M_{l-1}(i, j) < 0.5 \\ -\infty & \text{otherwise.} \end{cases} \quad (6)$$

The global masked-attention in Eq. (5) differs from the masked-attention by additionally attending to the background mask region, yet it retains the benefits of faster convergence w.r.t. the cross-attention.

3.3. Mask Contrastive Learning

The ideal characteristic of an anomaly segmentation model is to predict high anomaly scores for out-of-distribution (OOD) objects and low anomaly scores for in-distribution (ID) regions. Namely, we would like to have a significant margin between the likelihood of known classes being predicted at anomalous regions and vice-versa. A common strategy used to improve this separation is to fine-tune the model with auxiliary out-of-distribution (anomalous) data as supervision [21, 22, 4].

Here we propose a contrastive learning approach to encourage the model to have a significant margin between the anomaly scores for in-distribution and out-of-distribution classes. Our mask-based framework allows us to straightforwardly implement this contrastive strategy by using as supervision outlier images generated by cutting anomalous objects from the auxiliary OOD data and pasting it on top of the training data. For each outlier image, we can then generate a binary outlier mask M_{OOD} that is 1 for out-of-distribution pixels and 0 for in-distribution class pixels. With this setting, we first calculate the negative likelihood of in-distribution classes using the class scores C and class masks M as:

$$l_N = - \max_{k=1}^K (\text{softmax}(C)^T \cdot \text{sigmoid}(M)) \quad (7)$$



Figure 4: **Mask Refinement Illustration:** To obtain the refined prediction, we multiply the prediction map with a refinement mask that is built by assigning zero anomaly scores for pixels that are categorized as “stuff”, except for the “road”. The refinement eliminates many false positives at the boundary of objects and in the background. The region to be masked is white in the refinement mask.

Ideally, for pixels corresponding to in-distribution classes l_N should be -1 since the value of $\text{softmax}(C)^T$ and $\text{sigmoid}(M)$ would be close to 1. On the other hand, for an anomalous pixel, $\text{sigmoid}(M)$ is ideally 0 as M contains only inlier classes mask that results in l_N to be 0. Using l_N , we define our contrastive loss as:

$$L_{CL} = \frac{1}{2}(l_{CL}^2),$$

$$l_{CL} = \begin{cases} l_N & \text{if } M_{OOD} = 0 \\ \max(0, m - l_N) & \text{otherwise,} \end{cases} \quad (8)$$

where the margin m is a hyperparameter that decides the minimum distance between the out-of-distribution and in-distribution classes.

3.4. Refinement Mask

False positives are one of the main problems in anomaly segmentation, particularly around object boundaries. Hand-crafted methods such as iterative boundary suppression [27] or dilated smoothing have been proposed to minimize the false positives at boundaries or globally, however, they require tuning for each specific dataset. Instead, we propose a general refinement technique that leverages the capability of mask transformers [12] to perform all segmentation tasks. Our method stems from the panoptic perspective [28] that the elements in the scene can be categorized as *things*, *i.e.* countable objects, and *stuff*, *i.e.* amorphous regions. With this distinction in mind, we observe that in driving scenes, i) unknown objects are classified as things, and ii) they are often present on the road. Thus, we can proceed to remove most false positives by filtering out all the masks corresponding to “stuff”, except the “road” category. We implement this removal mechanism in the form of a binary refinement mask $R_M \in [0, 1]^{H \times W}$, which contains zeros in the segments corresponding to the unwanted “stuff” masks and one otherwise. Thus, by multiplying R_M with the predicted anomaly scores f we filter out all the unwanted “stuff” masks and eliminate a large portion of the false positives (see Fig. 4). Formally, for an image x the

refined anomaly scores f^r is computed as:

$$f^r(x) = R_M \odot f(x), \quad (9)$$

where \odot is the Hadamard product.

R_M is the dot product between the binarized output mask $\bar{M} \in \{0, 1\}^{N \times (H \times W)}$ and the class filter $\bar{C} \in \{0, 1\}^{1 \times N}$, *i.e.* $R_M = \bar{C} \cdot \bar{M}$. We define $\bar{M} = \text{sigmoid}(M) > 0.5$ and the class filter \bar{C} is equal to 1 only where the highest class score of $\text{softmax}(C)$ belongs to “things” or “road” classes and is greater than 0.95.

4. Experiments

Dataset: We train Mask2Anomaly on Cityscapes [14] and for evaluation we use Road Anomaly [34], Fishyscapes [3] and Segment Me If You Can (SMIYC) benchmarks [9].

Road Anomaly: is a collection of 60 web images having anomalous objects located on or near the road.

Fishyscapes (FS): consists of two datasets, Fishyscape static (FS static) and Fishyscapes lost & found (FS lost & found). Fishyscape static is built by blending Pascal VOC [19] objects on Cityscapes images containing 30 validation and 1000 test images. Fishyscapes lost & found is based on a subset of the Lost and Found dataset [42], with 100 validation and 275 test images.

SMIYC: consists of two datasets, RoadAnomaly21 (SMIYC-RA21) and RoadObstacle21 (SMIYC-RO21). The SMIYC-RA21 contains 10 validation and 100 test images with diverse anomalies. The SMIYC-RO21 is collected with a focus on segmenting road anomalies and has 30 validation and 327 test images.

Evaluation Metrics: We evaluate all the anomaly segmentation methods at pixel and component levels. For pixel-wise evaluation, we use Area under the Precision-Recall Curve (AuPRC) and False Positive Rate at a true positive rate of 95% (FPR₉₅). Since pixel-level evaluation metrics can neglect small anomalies and be biased towards anomalies with large sizes, we also include component-level evaluations using the averaged component-wise F1 ($F1^*$), the positive predictive value (PPV), and the component-wise intersection over union (sIoU). Further, details of all the metrics can be found in the supplementary material.

Implementation Details: Our implementation is derived from [13, 12]. We use a ResNet-50 [24] encoder, and its weights are initialized from a model that is pre-trained with barlow-twins [53] self-supervision on ImageNet [15]. We freeze the encoder weights during training, saving memory and training time. We use a multi-scale deformable attention Transformer (MSDeformAttn) [57] as the pixel decoder. The MSDeformAttn gives feature maps at 1/8, 1/16, and 1/32 resolution, providing image features to the transformer decoder layers. Our transformer decoder is adopted from [12] and consists of 9 layers with

Methods	SMIYC RA-21		SMIYC RO-21		FS L&F		FS Static		Road Anomaly		Average	
	AuPRC \uparrow	FPR ₉₅ \downarrow	AuPRC \uparrow	FPR ₉₅ \downarrow	AuPRC \uparrow	FPR ₉₅ \downarrow	AuPRC \uparrow	FPR ₉₅ \downarrow	AuPRC \uparrow	FPR ₉₅ \downarrow	AuPRC \uparrow	FPR ₉₅ \downarrow
Max Softmax [25](ICLR'17)	27.97	72.02	15.72	16.6	1.77	44.85	12.88	39.83	15.72	71.38	14.81	48.93
Entropy [25](ICLR'17)	-	-	-	-	2.93	44.83	15.4	39.75	16.97	71.1	11.66	51.89
Mahalanobis [30](NeurIPS'18)	20.04	86.99	20.9	13.08	-	-	-	-	14.37	81.09	18.42	60.38
Image Resynthesis [34](ICCV'19)	52.28	25.93	37.71	4.7	5.7	48.05	29.6	27.13	-	-	31.32	26.45
Learning Embedding [4](IJCV'21)	37.52	70.76	0.82	46.38	4.65	24.36	57.16	13.39	-	-	26.18	45.43
Void Classifier [4](IJCV'21)	36.61	63.49	10.44	41.54	10.29	22.11	4.5	19.4	-	-	15.46	36.63
JSRNet [49](ICCV'21)	33.64	43.85	28.09	28.86	-	-	-	-	94.4	9.2	52.04	47.3
SML [27](ICCV'21)	46.8	39.5	3.4	36.8	31.67	21.9	52.05	20.5	17.52	70.7	30.28	37.88
SynBoost [16](CVPR'21)	56.44	61.86	71.34	3.15	43.22	15.79	72.59	18.75	38.21	64.75	56.36	32.86
Maximized Entropy [10](ICCV'21)	<u>85.47</u>	15.00	85.07	0.75	29.96	35.14	86.55	8.55	48.85	31.77	<u>67.18</u>	18.24
Dense Hybrid [22](ECCV'22)	77.96	9.81	<u>87.08</u>	<u>0.24</u>	47.06	3.97	80.23	5.95	31.39	63.97	64.74	<u>16.79</u>
PEBEL [47](ECCV'22)	49.14	40.82	4.98	12.68	44.17	7.58	<u>92.38</u>	<u>1.73</u>	45.1	44.58	47.15	31.47
Mask2Anomaly (Ours)	88.7	<u>14.60</u>	93.3	0.20	<u>46.04</u>	<u>4.36</u>	95.20	0.82	<u>79.70</u>	<u>13.45</u>	80.59	6.68

Table 1: **Pixel level evaluation:** On average, Mask2Anomaly shows significant improvement among the compared methods. Higher values for AuPRC are better, whereas for FPR₉₅ lower values are better. The best and second best results are **bold** and underlined, respectively. ‘-’ indicates the unavailability of benchmark results.

Methods	SMIYC RA-21			SMIYC RO-21		
	sIoU \uparrow	PPV \uparrow	$F1^*$ \uparrow	sIoU \uparrow	PPV \uparrow	$F1^*$ \uparrow
Max Softmax [25](ICLR'17)	15.48	15.29	5.37	19.72	15.93	6.25
Ensemble [29](NurIPS'17)	16.44	20.77	3.39	8.63	4.71	1.28
Mahalanobis [30](NeurIPS'18)	14.82	10.22	2.68	13.52	21.79	4.70
Image Resynthesis [34](ICCV'19)	39.68	10.95	12.51	16.61	20.48	8.38
MC Dropout [41](CVPR'20)	20.49	17.26	4.26	5.49	5.77	1.05
Learning Embedding [4](IJCV'21)	33.86	20.54	7.90	35.64	2.87	2.31
SML [27](ICCV'21)	26.00	24.70	12.20	5.10	13.30	3.00
SynBoost [16](CVPR'21)	34.68	17.81	9.99	44.28	41.75	37.57
Maximized Entropy [10](ICCV'21)	49.21	<u>39.51</u>	28.72	<u>47.87</u>	<u>62.64</u>	48.51
JSRNet [49](ICCV'21)	20.20	29.27	13.66	18.55	24.46	11.02
Void Classifier [4](IJCV'21)	21.14	22.13	6.49	6.34	20.27	5.41
Dense Hybrid [22](ECCV'22)	<u>54.17</u>	24.13	<u>31.08</u>	45.74	50.10	<u>50.72</u>
PEBEL [47](ECCV'22)	38.88	27.20	14.48	29.91	7.55	5.54
Mask2Former [12]	25.20	18.20	15.30	5.00	21.90	4.80
Mask2Anomaly (Ours)	60.40	45.70	48.60	61.40	70.30	69.80

Table 2: **Component level evaluation:** Mask2Anomaly achieves large improvement on component level evaluation metrics among the baselined methods. Higher values of sIoU, PPV, and $F1^*$ are better. The best and second best results are **bold** and underlined, respectively.

100 queries. We train Mask2Anomaly using a combination of binary cross-entropy loss and the dice loss [40] for class masks and cross-entropy loss for class scores. The network is trained with an initial learning rate of 1e-4 and batch size of 16 for 90 thousand iterations on AdamW [38] with a weight decay of 0.05. We use an image crop of 380 \times 760 with large-scale jittering [18] along with a random scale ranging from 0.1 to 2.0.

Next, we train the Mask2Anomaly in a contrastive setting. We generate the outlier image using AnomalyMix [47] where we cut an object from MS-COCO [33] dataset image and paste them on the Cityscapes image. The corresponding binary mask for an outlier image is created by assigning 1 to the MS-COCO image area and 0 to the Cityscapes image area. We randomly sample 300 images from the MS-COCO dataset during training to generate outliers. We train the network for 4000 iterations with m as 0.75, a learning rate of 1e-5, and batch size 8, keeping all the other hyperparameters the same as above. The probability of choosing

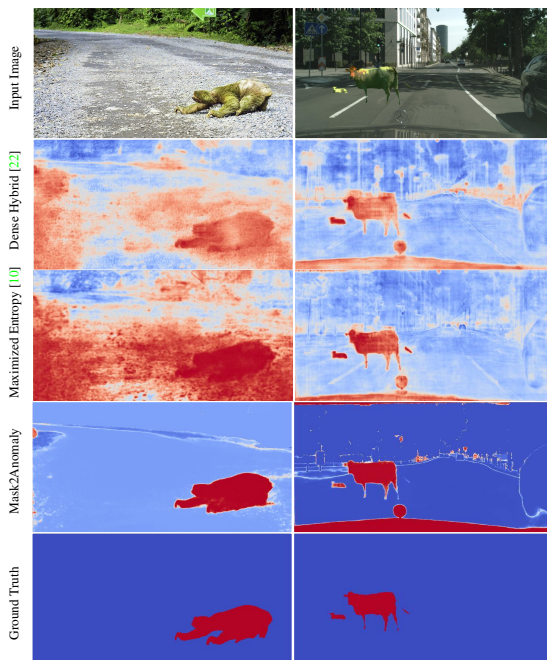


Figure 5: **Qualitative Results:** We observe that per-pixel classification architectures: Dense Hybrid [22] and Maximized Entropy [10] suffer from large false positives, whereas Mask2Anomaly, which is a mask-transformer, shows accurate pixel-wise anomaly segmentation results.

an outlier in a training batch is kept at 0.2.

4.1. Main Results

Table 1 shows the pixel-level anomaly segmentation results achieved by Mask2Anomaly and recent SOTA methods on Fishyscapes, SMIYC, and Road Anomaly datasets. We can observe that Mask2Anomaly significantly improves the average AuPRC by 20% and the FPR₉₅ by 60% compared to the second-best method. We observe that anomaly segmentation methods based on per-pixel architecture, such as JSRNet, perform exceptionally well on the Road

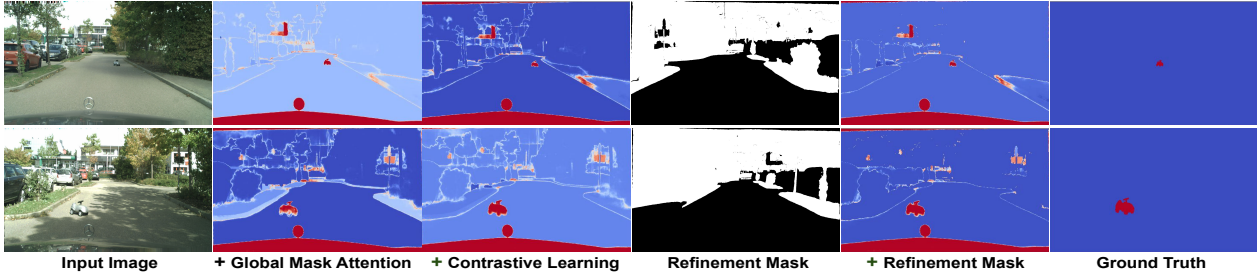


Figure 6: **Mask2Anomaly Qualitative Ablation**: demonstrates the performance gain by progressively adding (left to right) proposed components. Masked-out regions by refinement mask are shown in white. Anomalies are represented in red.

Anomaly dataset. However, JSRNet does not generalize well on other datasets. On the other hand, Mask2Anomaly yields excellent results on all the datasets. Moreover, the property of our mask architecture to encourage objectness, rather than individual pixel anomalies, not only reduces the false positive but also improves the localization of whole anomalies. Indeed, Tab. 2 demonstrates that Mask2Anomaly outperforms all the baselined methods on component-level evaluation metrics. To conclude, Mask2Anomaly yields state-of-the-art anomaly segmentation performance both in pixel and component metrics.

Qualitative results: To get a better understanding of the visual results, in Fig. 5 we visually compare the anomaly scores predicted by Mask2Anomaly and its closest competitors: Dense Hybrid [22] and Maximized Entropy [10]. The results from both: Dense Hybrid and Maximized Entropy exhibit a strong presence of false positives across the scene, particularly on the boundaries of objects (“things”) and regions (“stuff”). On the other hand, Mask2Anomaly demonstrates the precise segmentation of anomalies while at the same time having minimal false positives. Additional qualitative results are in the supplementary material.

Segmentation results: Another critical characteristic of any anomaly segmentation method is that it should not disrupt the in-distribution classification performance, or else it would make the semantic segmentation model unusable. We find that adding only GMA to the base model leads to in-distribution accuracy of 80.45 on the validation set of Cityscapes. The final Mask2Anomaly model maintains an in-distribution accuracy of 78.88 mIoU, which is still 1.46 points higher than the vanilla Mask2Former. Moreover, it is important to note that both Mask2Anomaly and Mask2Former are trained for 90k iterations, indicating that, although Mask2Anomaly additionally attends to the background mask region, it shows convergence similar to Mask2Former. Extended quantitative and qualitative segmentation results with both Mask2Anomaly and Mask2Former are presented in the supplementary material.

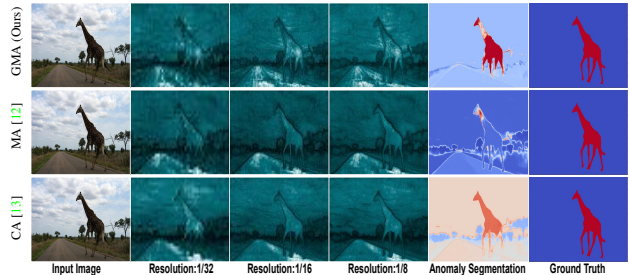


Figure 7: **Visualization of negative attention maps and results**: Global mask attention gives high attention scores to anomalous regions across all resolutions showing the best anomaly segmentation results among the compared attention mechanisms. Cross-attention performs better than mask-attention but has high false positives and low confidence prediction for the anomalous region. Darker regions represent low attention values. Details to calculate negative attention are given in Section:4.2.

4.2. Ablations

All the results reported in this section are from the Fishyscapes lost and found validation dataset.

Mask2Anomaly: Table 3(a) presents the results of a component-wise ablation of the technical novelties included in Mask2Anomaly. We use Mask2Former as the baseline. As shown in the table, removing any individual component from Mask2Anomaly drastically reduces the results, thus proving that their individual benefits are complimentary. In particular, we observe that the global masked attention has a big impact on the AuPRC and the contrastive learning is very important for the FPR₉₅. The mask refinement brings further improvements to both. Figure 6 visually demonstrates the positive effect of all the components.

Global Mask Attention: To better understand the effect of the global masked attention (GMA), in Tab. 3(c), we compare it to the masked-attention (MA) [12] and cross-attention (CA) [48]. We can observe that although the MA increases the mIoU w.r.t. the CA, it degrades all the metrics for anomaly segmentation, thus confirming our preliminary

					margin(m)	AuPRC \uparrow	FPR $_{95}\downarrow$	
	GMA	CL	RM	AuPRC \uparrow	FPR $_{95}\downarrow$	1	65.37	11.61
				<i>10.60</i>	<i>89.35</i>	0.95	65.40	12.20
	✓		✓	35.05	87.11	0.90	66.05	13.49
		✓	✓	57.23	31.93	0.80	66.20	14.89
	✓	✓		68.95	24.07	0.75	69.41	9.46
	✓	✓	✓	69.41	9.46	0.50	62.07	13.26

(a) (b)

				AuPRC \uparrow	FPR $_{95}\downarrow$	Batch Outlier Probability	AuPRC \uparrow	FPR $_{95}\downarrow$
	mIoU \uparrow	AuPRC \uparrow	FPR $_{95}\downarrow$	<i>68.95</i>	<i>24.07</i>	0.1	63.01	14.66
CA [13]	76.43	20.30	89.35	<i>w/o Refinement Mask</i>	<i>68.95</i>	<i>24.07</i>	0.2	69.41
MA [12]	77.42	10.60	89.39	$L_{\{things \setminus road\}}$	67.04	39.11	0.5	69.20
GMA	80.45	32.35	25.95	$L_{\{stuff \setminus road\}}$	69.41	9.46	1	68.77

(c) (d) (e)

Table 3: **Mask2Anomaly Ablation tables:** (a) Component-wise ablation of Mask2Anomaly. Results in *italics* show Mask2Former results. GMA: Global Mask Attention, CL: Contrastive Learning, and RM: Refinement Mask. (b) Shows the behavior of L_{CL} by choosing different margin(m) values. We empirically find the best results when m is 0.75. (c) Global masked attention (GMA) performs the best among various attention mechanisms: Cross-Attention (CA) and Masked-Attention (MA). (d) We show the performance gain by using a refinement mask that masks the $\{stuff \setminus road\}$ regions as anomalies are categorized as *things* class. (e) Batch outlier probability is the likelihood of selecting an outlier image for a batch during contrastive training. The best result is achieved at 0.2 probability. (All the results reported on FS Lost & Found validation set).

experiment shown in Fig. 3. On the other hand, the GMA provides improvements across all the metrics. This is confirmed visually in Fig. 7, where we show the negative attention maps for the three methods at different resolutions. The negative attention is calculated by averaging all the queries (since there is no reference known object) and then subtracting one. Note that the GMA has a high response on the anomaly (the giraffe) across all resolutions.

Refinement Mask: Table 3(d) shows the performance gains due to the refinement mask. We observe that filtering out the $\{“stuff” \setminus “road”\}$ regions of the prediction map improves the FPR $_{95}$ by 14.61 along with marginal improvement in AuPRC. On the other hand, removing the $\{“things” \setminus “road”\}$ regions degrades the results, confirming our hypothesis that anomalies are likely to belong to the “things” category. Figure 6 qualitatively shows the improvement achieved with the refinement mask. Also, refinement mask adds a small overhead of 1.12 GFlops compared to Mask2Anomaly 258 GFlops inference cost.

Mask Contrastive Learning: We tested the effect of the margin in the contrastive loss L_{CL} , and we report these results in Tab. 3(b). We find that the best results are achieved by setting m to 0.75, but the performance is competitive for any value of m in the table. Similarly, we tested the effect of the batch outlier probability, which is the likelihood of selecting an outlier image in a batch. The results shown in Tab. 3(e) indicate that the best performance is achieved at 0.2, but the results remain stable for higher values of the batch outlier probability.

Effect of bigger backbones: We demonstrate the effi-

Method	Backbone	AuPRC \uparrow	FPR $_{95}\downarrow$	FLOPs \downarrow	Training \downarrow Parameters
Mask2Former [12]	ResNet-50	10.60	89.35	226G	44M
	ResNet-101	9.11	45.83	293G	63M
	Swin-T	24.54	37.98	232G	42M
	Swin-S	30.96	36.78	313G	69M
Mask2Anomaly ‡	ResNet-50	32.35	25.95	258G	23M

Table 4: **Architectural Efficiency of Mask2Anomaly:** Mask2Anomaly outperforms the best Mask2Former architecture having Swin-S backbone with only 30% trainable parameters. Mask2Anomaly ‡ only uses global mask attention.

cacy of Mask2Anomaly by comparing it to the vanilla Mask2Former but using larger backbones. The results in Tab. 4 show that despite the disadvantage, Mask2Anomaly with a ResNet-50 still performs better than Mask2Former using large transformer-based backbones. It is also important to note that the number of training parameters for Mask2Anomaly can be reduced to 23M by using a frozen self-supervised pre-trained encoder, which is significantly less than all the Mask2Former variations.

5. Conclusion

In this work, we present Mask2Anomaly, a novel anomaly segmentation architecture established on masked architecture. Mask2Anomaly contains global mask attention specifically designed to improve the attention mechanism for anomaly segmentation tasks. Next, we develop a mask contrastive learning framework that utilizes outlier masks to maximize the separation between anomalies and

known classes. Finally, we introduced mask refinement that reduces false positives and improves the overall performance. We show the efficacy of Mask2Anomaly and its components through extensive qualitative and quantitative results. We hope Mask2Anomaly will open doors for new anomaly segmentation methods based on mask architecture.

References

- [1] Matt Angus, Krzysztof Czarnecki, and Rick Salay. Efficacy of pixel-level ood detection for semantic segmentation. *arXiv preprint arXiv:1911.02897*, 2019. [1](#)
- [2] Vijay Badrinarayanan, Alex Kendall, and Roberto Cipolla. Segnet: A deep convolutional encoder-decoder architecture for image segmentation. *IEEE TPAMI*, 39(12):2481–2495, 2017. [2](#)
- [3] Hermann Blum, Paul-Edouard Sarlin, Juan Nieto, Roland Siegwart, and Cesar Cadena. Fishyscapes: A benchmark for safe semantic segmentation in autonomous driving. In *Proceedings of the IEEE/CVF International Conference on Computer Vision Workshops*, pages 0–0, 2019. [1](#), [5](#)
- [4] Hermann Blum, Paul-Edouard Sarlin, Juan Nieto, Roland Siegwart, and Cesar Cadena. The fishyscapes benchmark: Measuring blind spots in semantic segmentation. *International Journal of Computer Vision*, 129(11):3119–3135, 2021. [2](#), [4](#), [6](#), [13](#)
- [5] Nicolas Carion, Francisco Massa, Gabriel Synnaeve, Nicolas Usunier, Alexander Kirillov, and Sergey Zagoruyko. End-to-end object detection with transformers. In *European conference on computer vision*, pages 213–229. Springer, 2020. [2](#), [3](#)
- [6] Jun Cen, Peng Yun, Junhao Cai, Michael Yu Wang, and Ming Liu. Deep metric learning for open world semantic segmentation. In *Proceedings of the IEEE/CVF International Conference on Computer Vision*, pages 15333–15342, 2021. [1](#)
- [7] Fabio Cermelli, Dario Fontanel, Antonio Tavera, Marco Ciccone, and Barbara Caputo. Incremental learning in semantic segmentation from image labels. In *CVPR*, pages 4371–4381, 2022. [1](#)
- [8] Fabio Cermelli, Massimiliano Mancini, Samuel Rota Bulò, Elisa Ricci, and Barbara Caputo. Modeling the background for incremental learning in semantic segmentation. In *CVPR*, 2020. [1](#)
- [9] Robin Chan, Krzysztof Lis, Svenja Uhlemeyer, Hermann Blum, Sina Honari, Roland Siegwart, Mathieu Salzmann, Pascal Fua, and Matthias Rottmann. Segmentmeifyoucan: A benchmark for anomaly segmentation. *arXiv preprint arXiv:2104.14812*, 2021. [2](#), [5](#), [12](#)
- [10] Robin Chan, Matthias Rottmann, and Hanno Gottschalk. Entropy maximization and meta classification for out-of-distribution detection in semantic segmentation. In *Proceedings of the IEEE/CVF International Conference on Computer Vision*, pages 5128–5137, 2021. [2](#), [6](#), [7](#), [13](#), [14](#), [16](#)
- [11] Liang-Chieh Chen, Yukun Zhu, George Papandreou, Florian Schroff, and Hartwig Adam. Encoder-decoder with atrous separable convolution for semantic image segmentation. In *Proceedings of the European conference on computer vision (ECCV)*, pages 801–818, 2018. [2](#), [3](#)
- [12] Bowen Cheng, Ishan Misra, Alexander G Schwing, Alexander Kirillov, and Rohit Girdhar. Masked-attention mask transformer for universal image segmentation. In *Proceedings of the IEEE/CVF Conference on Computer Vision and Pattern Recognition*, pages 1290–1299, 2022. [1](#), [2](#), [4](#), [5](#), [6](#), [7](#), [8](#), [15](#), [17](#)
- [13] Bowen Cheng, Alex Schwing, and Alexander Kirillov. Per-pixel classification is not all you need for semantic segmentation. *Advances in Neural Information Processing Systems*, 34:17864–17875, 2021. [2](#), [4](#), [5](#), [7](#), [8](#), [17](#)
- [14] Marius Cordts, Mohamed Omran, Sebastian Ramos, Timo Rehfeld, Markus Enzweiler, Rodrigo Benenson, Uwe Franke, Stefan Roth, and Bernt Schiele. The cityscapes dataset for semantic urban scene understanding. In *Proc. of the IEEE Conference on Computer Vision and Pattern Recognition (CVPR)*, 2016. [1](#), [5](#)
- [15] Jia Deng, Wei Dong, Richard Socher, Li-Jia Li, Kai Li, and Li Fei-Fei. Imagenet: A large-scale hierarchical image database. In *2009 IEEE conference on computer vision and pattern recognition*, pages 248–255. Ieee, 2009. [5](#)
- [16] Giancarlo Di Biase, Hermann Blum, Roland Siegwart, and Cesar Cadena. Pixel-wise anomaly detection in complex driving scenes. In *Proceedings of the IEEE/CVF conference on computer vision and pattern recognition*, pages 16918–16927, 2021. [2](#), [6](#), [12](#), [13](#)
- [17] Arthur Douillard, Yifu Chen, Arnaud Dapogny, and Matthieu Cord. Plop: Learning without forgetting for continual semantic segmentation. In *CVPR*, 2021. [1](#)
- [18] Xianzhi Du, Barret Zoph, Wei-Chih Hung, and Tsung-Yi Lin. Simple training strategies and model scaling for object detection. *arXiv preprint arXiv:2107.00057*, 2021. [6](#)
- [19] Mark Everingham, Luc Van Gool, Christopher KI Williams, John Winn, and Andrew Zisserman. The pascal visual object classes (voc) challenge. *International journal of computer vision*, 88(2):303–338, 2010. [5](#)
- [20] Dario Fontanel, Fabio Cermelli, Massimiliano Mancini, and Barbara Caputo. Detecting anomalies in semantic segmentation with prototypes. In *Proceedings of the IEEE/CVF Conference on Computer Vision and Pattern Recognition*, pages 113–121, 2021. [1](#), [2](#)
- [21] Matej Grcić, Petra Bevandić, and Siniša Šegvić. Dense open-set recognition with synthetic outliers generated by real nvp. *arXiv preprint arXiv:2011.11094*, 2020. [4](#)
- [22] Matej Grcić, Petra Bevandić, and Siniša Šegvić. Densehybrid: Hybrid anomaly detection for dense open-set recognition. In *European Conference on Computer Vision*, pages 500–517. Springer, 2022. [1](#), [2](#), [4](#), [6](#), [7](#), [12](#), [14](#), [16](#)
- [23] Kaiming He, Georgia Gkioxari, Piotr Dollár, and Ross Girshick. Mask r-cnn. In *Proceedings of the IEEE international conference on computer vision*, pages 2961–2969, 2017. [2](#)
- [24] Kaiming He, Xiangyu Zhang, Shaoqing Ren, and Jian Sun. Deep residual learning for image recognition. In *Proceedings of the IEEE conference on computer vision and pattern recognition*, pages 770–778, 2016. [5](#)
- [25] Dan Hendrycks and Kevin Gimpel. A baseline for detecting misclassified and out-of-distribution examples in neural networks. *arXiv preprint arXiv:1610.02136*, 2016. [1](#), [2](#), [3](#), [6](#), [12](#), [13](#)

- [26] Gao Huang, Zhuang Liu, Laurens Van Der Maaten, and Kilian Q Weinberger. Densely connected convolutional networks. In *Proceedings of the IEEE conference on computer vision and pattern recognition*, pages 4700–4708, 2017. 2
- [27] Sanghun Jung, Jungsoo Lee, Daehoon Gwak, Sungha Choi, and Jaegul Choo. Standardized max logits: A simple yet effective approach for identifying unexpected road obstacles in urban-scene segmentation. In *Proceedings of the IEEE/CVF International Conference on Computer Vision*, pages 15425–15434, 2021. 1, 2, 5, 6, 12
- [28] Alexander Kirillov, Kaiming He, Ross Girshick, Carsten Rother, and Piotr Dollár. Panoptic segmentation. In *Proceedings of the IEEE/CVF Conference on Computer Vision and Pattern Recognition*, pages 9404–9413, 2019. 2, 5
- [29] Balaji Lakshminarayanan, Alexander Pritzel, and Charles Blundell. Simple and scalable predictive uncertainty estimation using deep ensembles. *Advances in neural information processing systems*, 30, 2017. 6, 13
- [30] Kimin Lee, Kibok Lee, Honglak Lee, and Jinwoo Shin. A simple unified framework for detecting out-of-distribution samples and adversarial attacks. *Advances in neural information processing systems*, 31, 2018. 2, 6, 13
- [31] Shiyu Liang, Yixuan Li, and Rayadurgam Srikant. Enhancing the reliability of out-of-distribution image detection in neural networks. *arXiv preprint arXiv:1706.02690*, 2017. 2, 13
- [32] Guosheng Lin, Anton Milan, Chunhua Shen, and Ian Reid. Refinenet: Multi-path refinement networks for high-resolution semantic segmentation. In *CVPR*, 2017. 2
- [33] Tsung-Yi Lin, Michael Maire, Serge Belongie, James Hays, Pietro Perona, Deva Ramanan, Piotr Dollár, and C Lawrence Zitnick. Microsoft coco: Common objects in context. In *Computer Vision—ECCV 2014: 13th European Conference, Zurich, Switzerland, September 6–12, 2014, Proceedings, Part V 13*, pages 740–755. Springer, 2014. 6
- [34] Krzysztof Lis, Krishna Nakka, Pascal Fua, and Mathieu Salzmann. Detecting the unexpected via image resynthesis. In *Proceedings of the IEEE/CVF International Conference on Computer Vision*, pages 2152–2161, 2019. 1, 2, 5, 6, 13
- [35] Weitang Liu, Xiaoyun Wang, John Owens, and Yixuan Li. Energy-based out-of-distribution detection. *Advances in Neural Information Processing Systems*, 33:21464–21475, 2020. 12
- [36] Ziyin Liu, Zhikang Wang, Paul Pu Liang, Russ R Salakhutdinov, Louis-Philippe Morency, and Masahito Ueda. Deep gamblers: Learning to abstain with portfolio theory. *Advances in Neural Information Processing Systems*, 32, 2019. 12
- [37] Jonathan Long, Evan Shelhamer, and Trevor Darrell. Fully convolutional networks for semantic segmentation. In *CVPR*, 2015. 2
- [38] Ilya Loshchilov and Frank Hutter. Decoupled weight decay regularization. *arXiv preprint arXiv:1711.05101*, 2017. 6
- [39] Umberto Michieli and Pietro Zanuttigh. Continual semantic segmentation via repulsion-attraction of sparse and disentangled latent representations. In *Proceedings of the IEEE/CVF Conference on Computer Vision and Pattern Recognition*, pages 1114–1124, 2021. 1
- [40] Fausto Milletari, Nassir Navab, and Seyed-Ahmad Ahmadi. V-net: Fully convolutional neural networks for volumetric medical image segmentation. In *2016 fourth international conference on 3D vision (3DV)*, pages 565–571. Ieee, 2016. 3, 6
- [41] Jishnu Mukhoti and Yarin Gal. Evaluating bayesian deep learning methods for semantic segmentation. *arXiv preprint arXiv:1811.12709*, 2018. 1, 2, 6, 13
- [42] Peter Pinggera, Sebastian Ramos, Stefan Gehrig, Uwe Franke, Carsten Rother, and Rudolf Mester. Lost and found: detecting small road hazards for self-driving vehicles. In *2016 IEEE/RSJ International Conference on Intelligent Robots and Systems (IROS)*, pages 1099–1106. IEEE, 2016. 5
- [43] Matthias Rottmann, Pascal Colling, Thomas Paul Hack, Robin Chan, Fabian Hüger, Peter Schlicht, and Hanno Gottschalk. Prediction error meta classification in semantic segmentation: Detection via aggregated dispersion measures of softmax probabilities. In *2020 International Joint Conference on Neural Networks (IJCNN)*, pages 1–9. IEEE, 2020. 12
- [44] Aasheesh Singh, Aditya Kamireddypalli, Vineet Gandhi, and K Madhava Krishna. Lidar guided small obstacle segmentation. *arXiv preprint arXiv:2003.05970*, 2020. 14
- [45] Ruoqi Sun, Xinge Zhu, Chongruo Wu, Chen Huang, Jianping Shi, and Lizhuang Ma. Not all areas are equal: Transfer learning for semantic segmentation via hierarchical region selection. In *2019 IEEE/CVF Conference on Computer Vision and Pattern Recognition (CVPR)*, pages 4355–4364, 2019. 1
- [46] Antonio Tavera, Fabio Cermelli, Carlo Masone, and Barbara Caputo. Pixel-by-pixel cross-domain alignment for few-shot semantic segmentation. In *2022 IEEE/CVF Winter Conference on Applications of Computer Vision (WACV)*, pages 1959–1968, 2022. 1
- [47] Yu Tian, Yuyuan Liu, Guansong Pang, Fengbei Liu, Yuanhong Chen, and Gustavo Carneiro. Pixel-wise energy-biased abstention learning for anomaly segmentation on complex urban driving scenes. In *European Conference on Computer Vision*, pages 246–263. Springer, 2022. 1, 2, 6, 12
- [48] Ashish Vaswani, Noam Shazeer, Niki Parmar, Jakob Uszkoreit, Llion Jones, Aidan N Gomez, Łukasz Kaiser, and Illia Polosukhin. Attention is all you need. *Advances in neural information processing systems*, 30, 2017. 7
- [49] Tomas Vojir, Tomáš Šipka, Rahaf Aljundi, Nikolay Chumerin, Daniel Olmeda Reino, and Jiri Matas. Road anomaly detection by partial image reconstruction with segmentation coupling. In *Proceedings of the IEEE/CVF International Conference on Computer Vision*, pages 15651–15660, 2021. 1, 2, 6
- [50] Yingda Xia, Yi Zhang, Fengze Liu, Wei Shen, and Alan Yuille. Synthesize then compare: Detecting failures and anomalies for semantic segmentation. In *Proceedings of the European Conference on Computer Vision (ECCV)*, 2020. 1, 2, 12
- [51] Yingda Xia, Yi Zhang, Fengze Liu, Wei Shen, and Alan L. Yuille. Synthesize then compare: Detecting failures and

- anomalies for semantic segmentation. In *Computer Vision – ECCV 2020*, pages 145–161, 2020. 1
- [52] Yanchao Yang and Stefano Soatto. Fda: Fourier domain adaptation for semantic segmentation. In *2020 IEEE/CVF Conference on Computer Vision and Pattern Recognition (CVPR)*, pages 4084–4094, 2020. 1
- [53] Jure Zbontar, Li Jing, Ishan Misra, Yann LeCun, and Stéphane Deny. Barlow twins: Self-supervised learning via redundancy reduction. In *International Conference on Machine Learning*, pages 12310–12320. PMLR, 2021. 5
- [54] Junyi Zhang, Ziliang Chen, Junying Huang, Liang Lin, and Dongyu Zhang. Few-shot structured domain adaptation for virtual-to-real scene parsing. In *2019 IEEE/CVF International Conference on Computer Vision Workshop (ICCVW)*, pages 9–17, 2019. 1
- [55] Zhenli Zhang, Xiangyu Zhang, Chao Peng, Xiangyang Xue, and Jian Sun. Exfuse: Enhancing feature fusion for semantic segmentation. In *ECCV*, 2018. 2
- [56] Hengshuang Zhao, Jianping Shi, Xiaojuan Qi, Xiaogang Wang, and Jiaya Jia. Pyramid scene parsing network. In *CVPR*, 2017. 2
- [57] Xizhou Zhu, Weijie Su, Lewei Lu, Bin Li, Xiaogang Wang, and Jifeng Dai. Deformable detr: Deformable transformers for end-to-end object detection. *arXiv preprint arXiv:2010.04159*, 2020. 5

Supplementary Material

Summary: This supplementary material contains additional method explanations, experiments, and results of Mask2Anomaly that include:

- explanation of anomaly segmentation evaluation metrics;
- Mask2Anomaly results on validation sets;
- outlier loss comparison and analysis;
- training loss functions of Mask2Anomaly ;
- an analysis of various inference techniques applied to a Mask2Anomaly;
- performance stability of Mask2Anomaly;
- additional results and supplementary video.

A. Evaluation Metrics

Pixel-Level: For pixel-wise evaluation, consider $Y \in \{Y_a, Y_{na}\}$ is the pixel level annotated ground truth labels for image χ containing anomaly. Y_a and Y_{na} represents the anomalous and non-anomalous labels in the ground-truth. Assume, $\hat{Y}(\gamma)$ is the model prediction obtained at thresholding $f(x)$ at γ . Then, we can write precision and recall equations as:

$$\text{precision}(\gamma) = \frac{|Y_a \cap \hat{Y}_a(\gamma)|}{|\hat{Y}_a(\gamma)|} \quad (10)$$

$$\text{recall}(\gamma) = \frac{|Y_a \cap \hat{Y}_a(\gamma)|}{|Y_a|} \quad (11)$$

and, AuPRC can be approximated as:

$$\text{AuPRC} = \int_{\gamma} \text{precision}(\gamma) \text{recall}(\gamma) \quad (12)$$

The AuPRC works well for unbalanced datasets making it particularly suitable for anomaly segmentation since all the datasets are significantly skewed. Next, we consider the False Positive Rate at a true positive rate of 95% (FPR_{95}), an important criterion for safety-critical applications that is calculated as:

$$\text{FPR}_{95} = \frac{|\hat{Y}_a(\gamma^*) \cap Y_{na}|}{|Y_{na}|} \quad (13)$$

where γ^* is a threshold when the true positive rate is 95%.

Component-Level: SMIYC [9] introduced a few component-level evaluation metrics that solely focus on detecting anomalous objects regardless of their size. These metrics are important to be considered because pixel-level metrics may not penalize a model for missing a small anomaly, even though such a small anomaly may be important to be detected. In order to have a component-level assessment of the detected anomalies, the quantities to be considered are the component-wise true-positives (TP),

Methods	FS L&F		FS static	
	AuPRC \uparrow	FPR $_{95}$ \downarrow	AuPRC \uparrow	FPR $_{95}$ \downarrow
Max Softmax [25]	4.59	40.59	19.09	23.99
Max Logit [25]	14.59	42.21	38.64	18.26
Entropy [25]	10.36	40.34	26.77	23.31
Energy [35]	25.79	32.26	31.66	37.32
SynthCP [50]	6.54	45.95	23.22	34.02
SynBoost [16]	40.99	34.47	48.44	47.71
SML [27]	36.55	14.53	48.67	16.75
Deep Gambler [36]	39.77	12.41	67.69	15.39
Dense Hybrid [22]	<u>63.80</u>	6.10	60.20	<u>4.90</u>
PEBEL [47]	59.83	<u>6.49</u>	<u>82.73</u>	6.81
Mask2Anomaly (Ours)	69.41	9.46	90.54	1.98

Table 5: **Fishyscapes Validation Results:** The best and second best results are **bold** and underlined, respectively.

false-negatives (FN), and false-positives (FP). These component-wise quantities can be measured by considering the anomalies as the positive class. From these quantities, we can use three metrics to evaluate the component-wise segmentation of anomalies: $sIoU$, PPV , and $F1^*$. Here we provide the details of how these metrics are computed, using the notation \mathcal{K} to denote the set of ground truth components, and $\hat{\mathcal{K}}$ to denote the set of predicted components.

The $sIoU$ metric used in SMIYC [9] is a modified version of the component-wise intersection over union proposed in [43], which considers the ground-truth components in the computation of the TP and FN . Namely, it is computed as

$$sIoU(k) = \frac{|k \cap \hat{K}(k)|}{|k \cap \hat{K}(k) \setminus \mathcal{A}(k)|}, \quad \hat{K}(k) = \bigcup_{\hat{k} \in \hat{\mathcal{K}}, \hat{k} \cap k \neq \emptyset} \hat{k} \quad (14)$$

where $\mathcal{A}(k)$ is an adjustment term that excludes from the union those pixels that correctly intersect with another ground-truth component different from k . We refer the reader to [9] for more details on this term. Given a threshold $\tau \in [0, 1]$, a target $k \in \mathcal{K}$ is considered a TP if $sIoU(k) > \tau$, and a FN otherwise.

The positive predictive value (PPV) is a metric that measures the FP for a predicted component $\hat{k} \in \hat{\mathcal{K}}$, and it is computed as

$$PPV(\hat{k}) = \frac{|\hat{k} \cap \hat{K}(k)|}{|\hat{k}|} \quad (15)$$

A predicted component $\hat{k} \in \hat{\mathcal{K}}$ is considered a FP if $PPV(\hat{k}) \leq \tau$. Finally, the $F1^*$ summarizes all the component-wise TP , FN , and FP quantities by the following formula:

$$F1^*(\tau) = \frac{2TP(\tau)}{2TP(\tau) + FN(\tau) + FP(\tau)} \quad (16)$$

B. Results on Fishyscapes and SMIYC validation sets

To provide a comprehensive evaluation, we have benchmarked Mask2Anomaly results on the Fishyscapes and

Methods	SMIYC-RA21		SMIYC-RO21	
	AuPRC \uparrow	FPR $_{95}$ \downarrow	AuPRC \uparrow	FPR $_{95}$ \downarrow
Max Softmax [25]	40.4	60.2	43.4	3.8
ODIN [31]	46.3	61.5	46.6	4.0
Mahalanobis [30]	22.5	86.4	25.9	26.1
MC Dropout [41]	29.2	77.9	7.9	43.8
Ensemble [29]	16.0	80.0	4.7	98.3
Void Classifier [4]	39.3	66.1	9.8	43.6
Learning Embedding [4]	51.9	60.0	1.5	56.7
Image Resynthesis [34]	76.4	20.5	70.3	1.3
SynBoost [16]	68.8	30.9	81.4	2.8
Maximized Entropy [10]	<u>80.7</u>	<u>17.4</u>	94.4	0.4
Mask2Anomaly (Ours)	94.5	3.3	<u>88.6</u>	0.3

Table 6: **SMIYC Validation Results:** The best and second best results are **bold** and underlined, respectively.

SMIYC validation sets as presented in Tab. 5 and Tab. 6, respectively. We can observe that Mask2Anomaly outperforms all the prior methods by a large margin on both benchmarks. Interestingly, maximized entropy and dense hybrid show the best AuPRC for SMIYC-RO21 and FPR $_{95}$ for FS L&F, respectively. However, overall Mask2Anomaly gives the best performance on all the benchmarks. This suggests that mask-based architecture offers better generalizability in comparison to per-pixel architecture due to its intrinsic property of encouraging objectness.

C. Outlier Loss Comparison

We now empirically demonstrate why mask contrastive loss, a margin-based loss, performs better at anomaly segmentation than binary cross-entropy loss. We train Mask2Anomaly with M_{OOD} using binary-cross entropy. The new loss based on the binary cross entropy can be written as:

$$L_{BCE} = M_{OOD} \log(l_N) + (1 - M_{OOD}) \log(1 - l_N) \quad (17)$$

$$\text{where, } l_N = -\max_{k=1}^K (\text{softmax}(C)^T \cdot \text{sigmoid}(M)) \quad (18)$$

l_N is the negative likelihood of in-distribution classes calculated using the class scores C and class masks M . Figure 8 illustrates the anomaly segmentation performance comparison on FS L&F validation dataset between the Mask2Anomaly when trained with the binary cross entropy loss and mask contrastive loss, respectively. We can observe that the mask contrastive loss achieves a wider margin between out-of-distribution(anomaly) and in-distribution prediction while maintaining significantly lower false positives.

D. Training Loss

Mask2Anomaly gives two sets of outputs: class scores (C) and class masks (M). To train M , we first pad the ground truth mask M^{gt} with “no object” masks denoted by ϕ . Since we assume $M \geq M^{gt}$, padding the ground truth masks allow us one-to-one matching. Now, we use bipartite match-

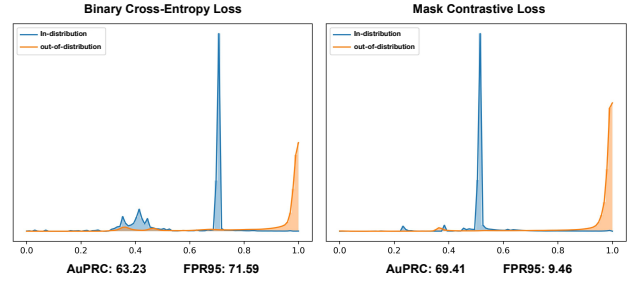


Figure 8: **Outlier Loss Comparison:** To train Mask2Anomaly on the outlier set, we find that mask contrastive loss, which is a margin-based loss shows better performance compared to the binary cross-entropy loss. Both experiments are done on the FS L&F validation set.

ing to match the ground truth and the predicted masks, and the assignment cost is given by:

$$L_{masks} = \lambda_{bce} L_{bce} + \lambda_{dice} L_{dice} \quad (19)$$

where L_{bce} and L_{dice} are the binary cross entropy loss and the dice loss calculated between the matched masks. λ_{bce} and λ_{dice} are the loss weights that are both set to 5.0. To train C , which indicates the semantic class of a mask, we used the cross-entropy loss L_{ce} . The total training loss is given by:

$$L = L_{masks} + \lambda_{ce} L_{ce} \quad (20)$$

with λ_{ce} set to 2.0 for the prediction that matched with ground truth and 0.1 for ϕ , *i.e.* for no object. After training the Mask2Anomaly for 90K iterations, we fine-tune the network with the mask contrastive loss L_{CL} . The new training loss is written as:

$$L_{M2A} = L + L_{CL} \quad (21)$$

We perform all the training and inference on a single Nvidia Titan RTX with 24GB memory.

E. Mask2Anomaly Inference

The per-pixel classification networks have a straightforward inference as the network outputs a pixel-wise anomaly map. However, in the case of a mask architecture, we get a set of class scores C and a set of binary mask M . So, we test various inference techniques on Mask2Anomaly for anomaly segmentation, as shown in Table 7. We find that the marginalization over class scores obtained after the softmax and taking the sigmoid of the mask yields the best results. Also, we observe that applying a softmax after the marginalization to perform max-softmax [25] does not give good results.

C	M	$f(C), f(M)$	SMIYC-RA21		SMIYC-RO21		FS L&F		FS Static		Road Anomaly		Average	
			AuPRC \uparrow	FPR ₉₅ \downarrow	AuPRC \uparrow	FPR ₉₅ \downarrow	AuPRC \uparrow	FPR ₉₅ \downarrow	AuPRC \uparrow	FPR ₉₅ \downarrow	AuPRC \uparrow	FPR ₉₅ \downarrow	AuPRC \uparrow	FPR ₉₅ \downarrow
I	I	I	9.47	95.16	4.44	73.45	2.53	92.16	1.18	99.97	65.59	97.56	16.64	91.66
Softmax	Softmax	I	44.73	38.27	3.16	95.72	4.82	47.98	10.34	52.04	42.74	55.73	21.13	57.94
Sigmoid	Sigmoid	I	25.04	93.14	83.14	1.24	14.55	43.83	45.67	96.87	28.1	91.63	39.3	65.34
Sigmoid	Softmax	I	29.29	39.01	7.48	98.01	0.42	48.23	6.37	52.16	25.61	55.78	13.83	58.63
Softmax	Sigmoid	I	95.48	2.41	92.89	0.15	69.41	9.46	90.54	1.98	79.7	13.45	85.56	5.51
Softmax	Sigmoid	Softmax	94.55	3.31	88.59	0.36	70.8	32.66	88.96	2.22	78.3	15.54	84.24	10.81

Table 7: **Mask2Anomaly Inference**: we show various inference techniques on Mask2Anomaly for anomaly segmentation. $f(\cdot)$ represents the function applied to class scores or masks. I is the identity function. The best results are in bold.

Methods	SMIYC-RA21		SMIYC-RO21		FS L&F		FS Static		Average σ	
	AuPRC \uparrow	FPR ₉₅ \downarrow	AuPRC \uparrow	FPR ₉₅ \downarrow	AuPRC \uparrow	FPR ₉₅ \downarrow	AuPRC \uparrow	FPR ₉₅ \downarrow	AuPRC	FPR ₉₅
Mask2Anomaly-S1	95.48	2.41	92.89	0.15	69.41	9.46	90.54	1.98	-	-
Mask2Anomaly-S2	92.03	3.22	92.3	0.27	69.19	13.47	85.63	5.06	-	-
σ (Mask2Anomaly)	± 2.44	± 0.57	± 0.42	± 0.08	± 0.16	± 2.84	± 3.47	± 2.18	± 1.62	± 1.41
Dense Hybrid-S1	52.99	38.87	66.91	1.91	56.89	8.92	52.58	6.03	-	-
Dense Hybrid-S2	60.59	32.14	79.64	1.01	47.97	18.35	54.22	5.24	-	-
σ (Dense Hybrid)	± 5.37	± 4.76	± 9.00	± 0.64	± 6.31	± 6.67	± 1.16	± 0.56	± 5.46	± 3.15

Table 8: **Performance stability in Mask2Former**: we can observe that the average deviation in the performance of the dense hybrid is significantly higher than Mask2Anomaly. σ denotes the standard deviation.

F. Performance stability on different outlier sets

Employing an outlier set to train an anomaly segmentation model presents a challenge because the model’s performance can vary significantly across different sets of outliers. Here, we show that Mask2Anomaly performs similarly when trained on different outlier sets.

We randomly chose two subsets of 300 MS-COCO images (S1, S2) as our outlier dataset for training Mask2Anomaly and DenseHybrid. Table 8 shows the performance of Mask2Anomaly and Dense Hybrid trained on S1 and S2 outlier sets, along with the standard deviation(σ) in the performance. We can observe that the variation in performance for the dense hybrid is significantly higher than Mask2Anomaly. Specifically, in dense hybrid, the average deviation in AuPRC is greater than 300%, and the average variation in FPR₉₅ is more than 200% compared to Mask2Anomaly.

G. Additional Results

Segmentation results: In Tab. 9 and Fig. 9, we show the segmentation results for Mask2Anomaly and Mask2Former. We can qualitatively and qualitatively infer that Mask2Anomaly performs better than Mask2Former.

Qualitative anomaly segmentation: In Fig. 10, we show the qualitative comparison of Mask2Anomaly with best-existing anomaly segmentation methods: Maximized Entropy [10] and Dense Hybrid [22]. We observe that these per-pixel classification architectures suffer from large false positives, whereas Mask2Anomaly, a mask-transformer, shows confident results across all datasets.

Attention comparison: Figure 11 shows the anomaly segmentation results obtained using various attention

mechanisms, and the global mask attention clearly exhibits the best performance.

Qualitative ablation study: We show a component-wise qualitative ablation of Mask2Anomaly in Fig. 12 by progressively adding each components. We can observe that each proposed component improves anomaly segmentation and complements the others.

Supplementary video: Shows the performance of Mask2Anomaly on the sequence of images of small obstacle dataset [44]. Mask2Anomaly displays an impressive performance in segmenting wildlife on the road and anomalies in low-light conditions.

Failure cases: Fig. 13 shows that Mask2Anomaly struggles to segment tiny anomalies and falsely detects road potholes as anomalies.

Methods	road	s. walk	building	wall	fence	pole	t. light	t. sign	veg.	terrain	sky	person	rider	car	truck	bus	train	mbike	bicycle	mIoU
Mask2Former	98.4	87.0	92.7	46.1	59.9	69.5	75.3	82.2	92.9	63.8	95.2	84.9	69.3	95.6	58.7	77.0	79.9	62.7	80.0	77.4
Mask2Anomaly	98.5	86.3	91.5	53.9	60.2	67.5	74.3	88.1	93.1	62.6	96	84.1	62.7	95.7	79.6	80.3	77.1	70.1	77.1	78.8

Table 9: Class-wise semantic segmentation results comparison between Mask2Former and Mask2Anomaly on Cityscapes validation set.

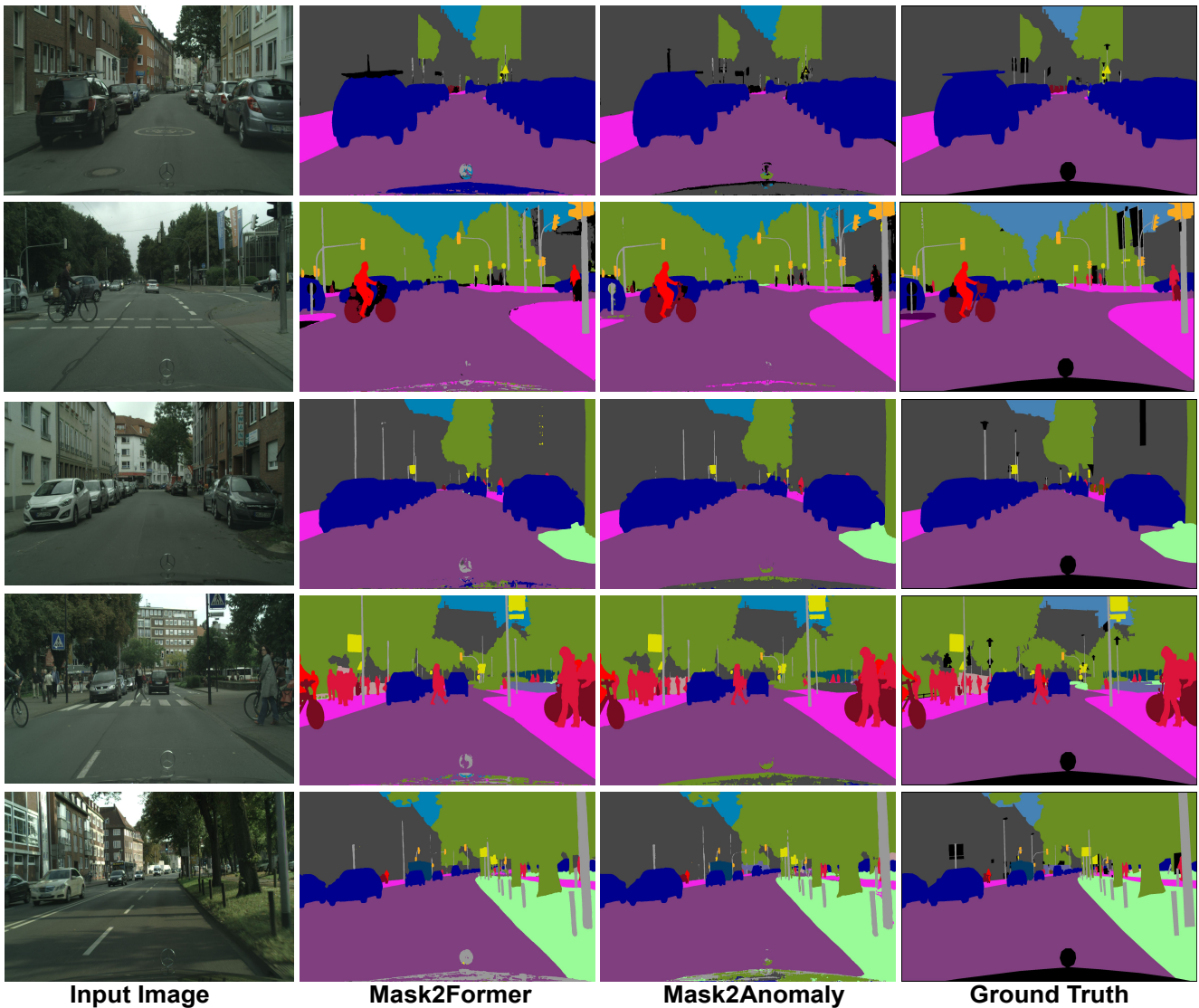
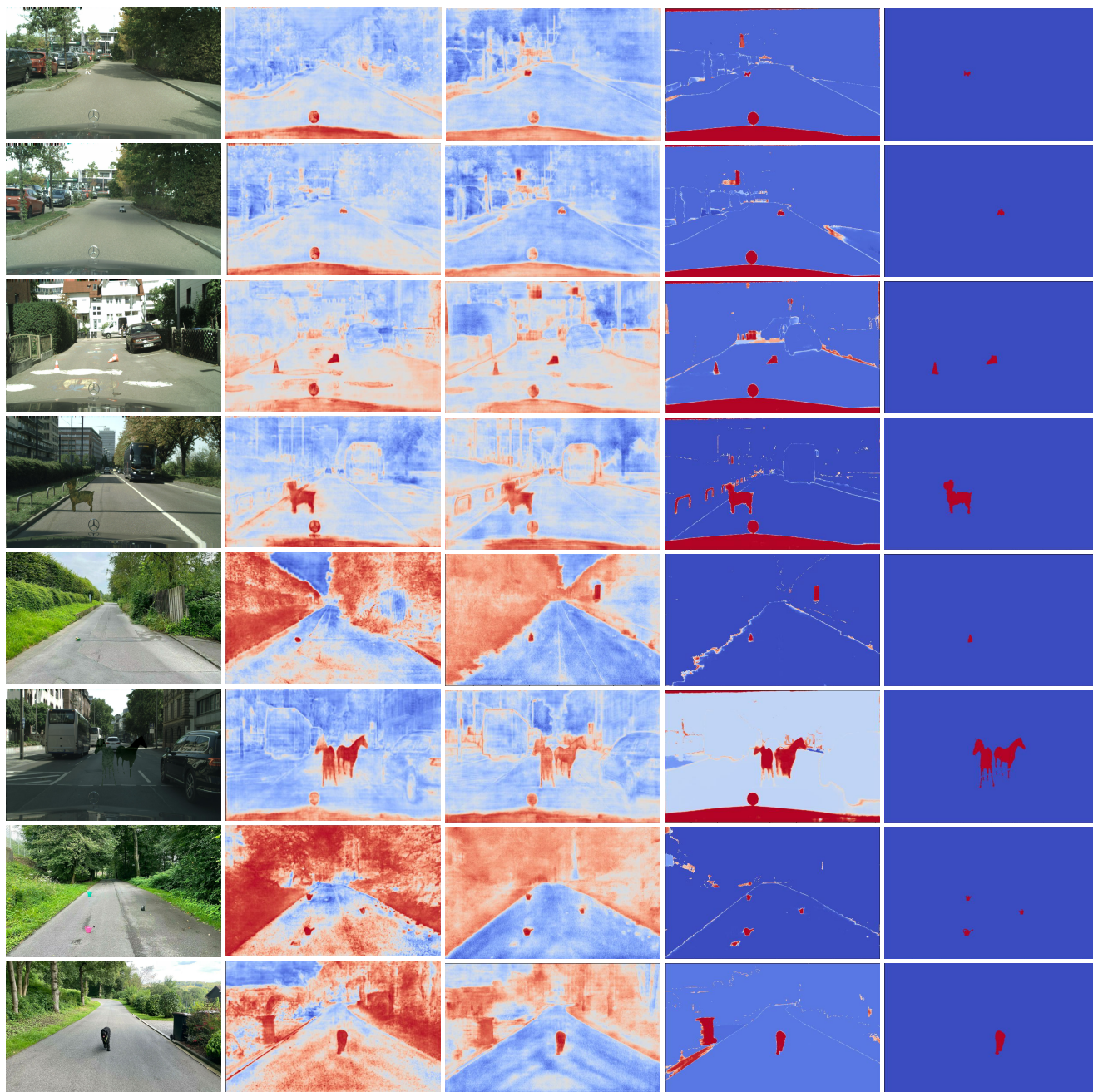


Figure 9: **Semantic Segmentation Results:** We can visually infer that Mask2Anomaly shows similar segmentation results when compared with Mask2Former [12].



Input Image Maximized Entropy [10] Dense Hybrid [22] Mask2Anomaly(Ours) Ground Truth

Figure 10: **Qualitative Results:** We observe that per-pixel classification architecture: Maximized Entropy and Dense Hybrid suffer from large false positives, whereas Mask2Anomaly which is a mask-transformer, show confident results across all datasets. Anomalies are represented in red.

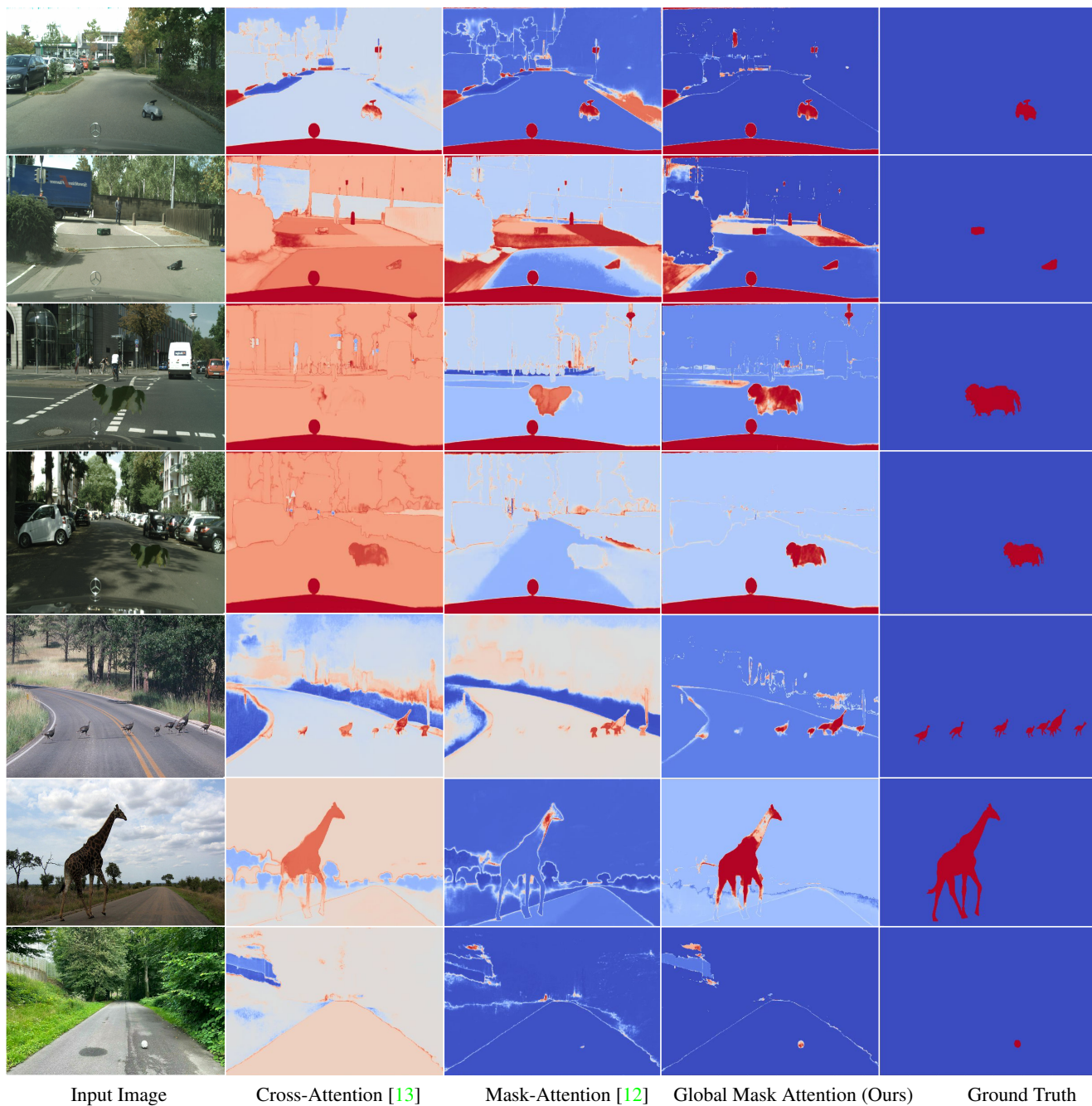


Figure 11: **Attention Comparison:** We observe that the proposed global mask attention can better segment anomaly among the compared attention mechanism. Anomalies are represented in red.

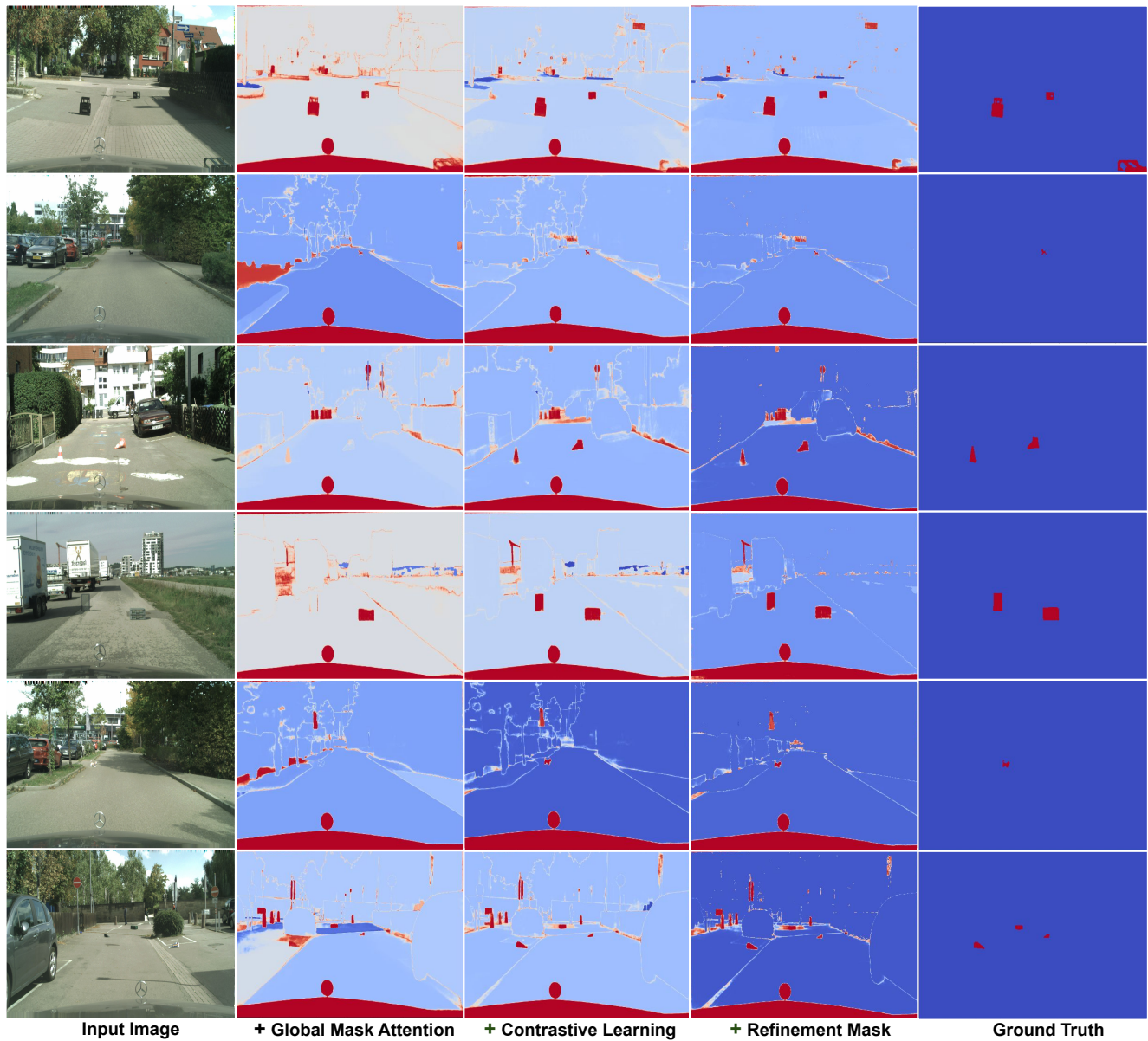


Figure 12: **Mask2Anomaly Qualitative Ablation**: shows the performance gain by progressively adding (left to right) proposed components. Anomalies are represented in red.

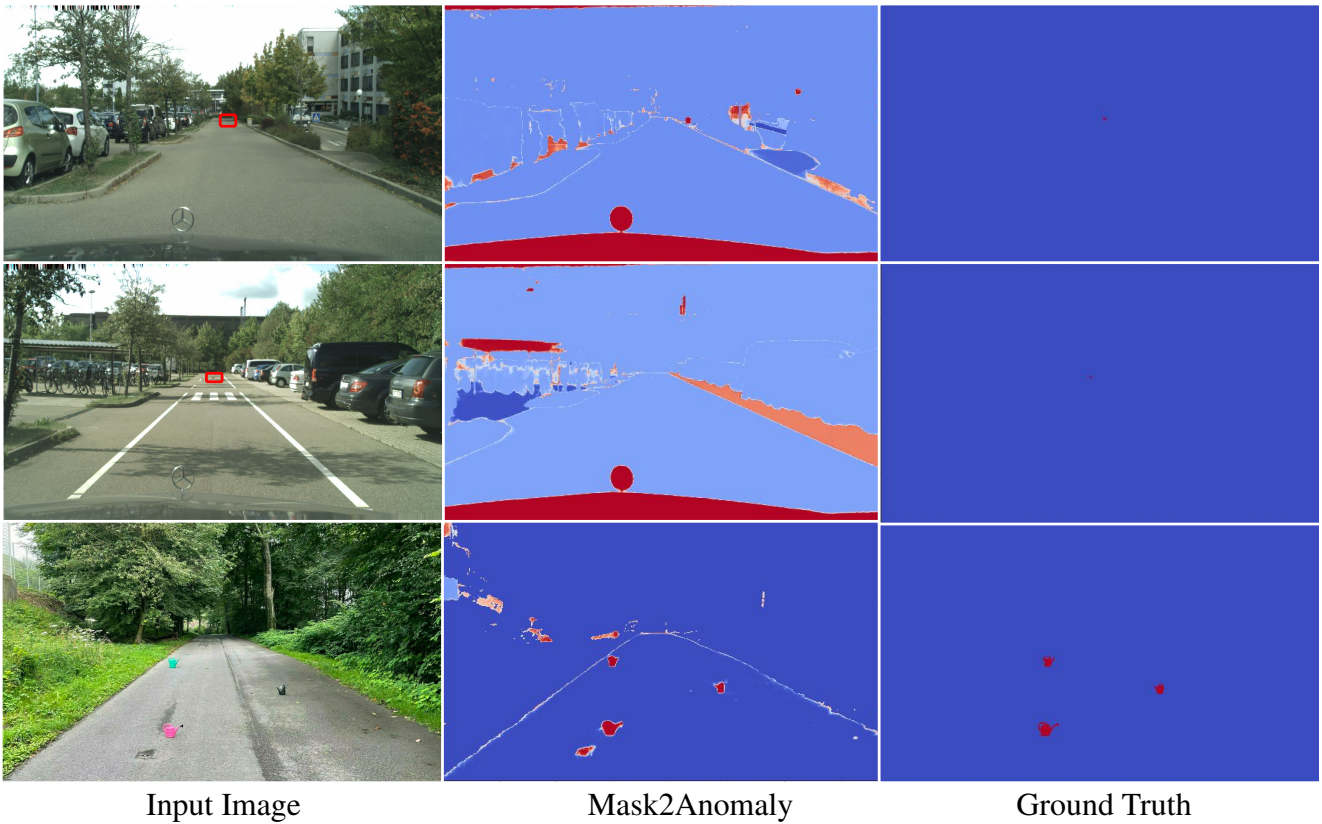


Figure 13: **Failure Cases:** Row (1,2): We can observe that Mask2Anomaly is unable to segment tiny anomalies (inside red bounding boxes of input image). Please zoom in for better clarity. Row 3: Mask2Anomaly falsely segments the pothole on the road as an anomaly. Anomalies are indicated in red in the ground truth.